JOURNAL OF SYNCHROTRON RADIATION

ISSN 1600-5775

Angular vibrations of cryogenically cooled double-crystal monochromators

I. Sergueev,* R. Döhrmann, J. Horbach and J. Heuer

Deutsches Elektronen-Synchrotron, D-22607 Hamburg, Germany. *Correspondence e-mail: ilya.sergeev@desy.de

Received 15 March 2016
Accepted 8 July 2016

Edited by G. E. Ice, Oak Ridge National Laboratory, USA

Keywords: X-ray optics; monochromator; compound refractive lens.

The effect of angular vibrations of the crystals in cryogenically cooled monochromators on the beam performance has been studied theoretically and experimentally. A simple relation between amplitude of the vibrations and size of the focused beam is developed. It is shown that the double-crystal monochromator vibrations affect not only the image size but also the image position along the optical axis. Several methods to measure vibrations with the X-ray beam are explained and analyzed. The methods have been applied to systematically study angular crystal vibrations at monochromators installed at the PETRA III light source. Characteristic values of the amplitudes of angular vibrations for different monochromators are presented.

1. Introduction

The current trend in the development and upgrade of synchrotron radiation sources is to provide nano-scale spatial resolution of the X-ray beam for routine experiments with different methods used at the facilities. Such a development requires a decrease of the X-ray source size and extreme performance of the X-ray optics, which often includes a double-crystal high-heat-load monochromator (DCM) as a main element. The ideal monochromator must preserve the coherence of the X-ray beam passing through. Practically, the wavefront of the beam is always perturbed due to static and dynamical sources. The curvature of the crystal surface introduced either by clamping in the crystal cage or by heat-load is the static source of perturbation. The effect of the heat-load on monochromator performance has been intensively studied during the last years theoretically and experimentally (Chumakov *et al.*, 2004; Rutishauser *et al.*, 2013; Zhang *et al.*, 2013; Huang *et al.*, 2014; Chumakov *et al.*, 2014). It has been shown that the slope error $\Delta\theta$ of the crystal surface leads to an increase of the virtual X-ray source by $\Delta z = 2L\Delta\theta$, where L is the distance from the monochromator to the source. Thus, the slope error of 1 µrad leads, for L = 30 m, to the source broadening by 60 µm, which is larger than the source size.

Cryogenic cooling by liquid nitrogen is used in order to decrease the effect of heat-load on the first crystal of the monochromator (Bilderback *et al.*, 2000). However, this cooling method often is a source of dynamical perturbations of the X-ray beam shape due to the induced angular vibrations of the monochromator crystals. Beside the cryogenic cooling, other sources can lead to angular vibrations, in particular the feedback system which is often used to keep the Bragg angle in the correct position. The monochromator vibrations worsen the X-ray beam quality and lead to the deterioration of the experimental results (Hinebaugh *et al.*, 2012; Uhlén *et al.*, 2014). The vibrations of particular monochromators were

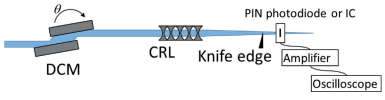

investigated in several studies (Yamazaki *et al.*, 2013; Chumakov *et al.*, 2014; Zozulya *et al.*, 2014; Kristiansen *et al.*, 2015).

Here, we present a theoretical and experimental investigation of the effect of monochromator angular vibrations on the X-ray beam properties. The theoretical definition of these vibrations is introduced in the first part and the effect of the vibrations on the properties of the focused X-ray beam is analyzed in the phase-space approach. It is shown that vibrations lead to the broadening of the focal spot and the relations between amplitude of vibrations and beam size are established. In addition, we found that the image position along the optical axis is also affected by vibrations. This effect is significant for the long-focal-length lens. A description of the experimental setup for the measurements of monochromator vibrations is presented in the second part. This method has been applied to study vibrations of the monochromators installed at the PETRA III light source. An overview of the results obtained with a description of the characteristic amplitudes of vibrations and their sources is presented in the last part of the paper.

2. Theoretical description of monochromator vibrations

Here, we consider the double-crystal monochromator (DCM) with the same symmetric Bragg reflections for two crystals in the non-dispersive geometry. The distance between crystals is usually much smaller than the distance from the monochromator to the X-ray source. Thus, in the theoretical model, we ignore the distance between crystals and assume that both reflections occur at the same point. The time-dependent angular vibrations of the first and second crystals around the equilibrium position are described by the functions $\varphi_{m1}(t)$ and $\varphi_{m2}(t)$, respectively, as shown in Fig. 1. The total DCM angular vibrations are defined as $\varphi_m(t) = \varphi_{m1}(t) - \varphi_{m2}(t)$, so that the change of the beam direction after the DCM is $2\varphi_m(t)$. We assume that the amplitude of the vibrations is smaller than the width of the rocking curve of the monochromator, so that the X-ray flux passing through the DCM is not affected by variation of φ_m. This assumption is valid for the vibrations with characteristic amplitude of about 0.1–1 µrad and Si(111) reflections chosen for the DCM crystals at an energy in the range 10–30 keV, which are typical conditions for many monochromators.

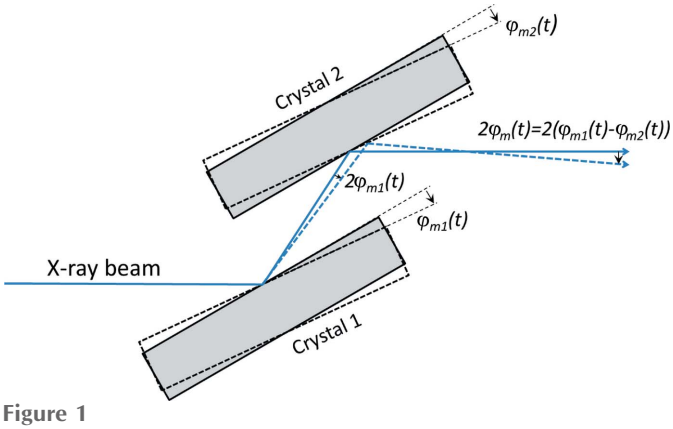

Figure 1
Schematic diagram of the angles of vibrations for the DCM.

We characterize the DCM angular vibrations *via* root-mean-square (RMS) deviation, σ_m, from the equilibrium position,

$$\sigma_m^2 = \langle \varphi_m^2(t) \rangle = \frac{1}{T} \int_0^T \mathrm{d}t\, \varphi_m^2(t), \tag{1}$$

where brackets denote the average over time, T is the time value much larger than the characteristic vibrations periods and the mean value of $\varphi_m(t)$ is assumed to be zero, *i.e.* $\langle \varphi_m(t) \rangle = 0$. Equation (1) includes the difference of two angles and can be written as

$$\begin{aligned} \sigma_m^2 &= \left\langle \left[\varphi_{m1}(t) - \varphi_{m2}(t) \right]^2 \right\rangle \\ &= \langle \varphi_{m1}^2(t) \rangle + \langle \varphi_{m2}^2(t) \rangle - 2 \langle \varphi_{m1}(t) \varphi_{m2}(t) \rangle, \end{aligned} \tag{2}$$

which includes the RMS values of the angular vibrations of the first and second crystals and the correlation between them. The contribution of the correlation part depends on the type of the monochromator. The vibrations of both crystals are almost anti-correlated for the channel-cut monochromator where $\varphi_{m1}(t) \approx \varphi_{m2}(t)$ and $\sigma_m \approx 0$. On the other hand, the correlation part almost disappears for a long-arm monochromator with individual angular stages for the crystals, where $\sigma_m^2 \approx \langle \varphi_{m1}^2(t) \rangle + \langle \varphi_{m2}^2(t) \rangle$. The crystal vibrations in the other types of monochromators usually include partial correlations between vibrations of individual crystals depending on the vibration frequency.

The relative influence of the monochromator angular vibrations on the unfocused beam is small and can often be neglected. The vertical deviation of the direct beam due to the vibrations is equal to $2\sigma_m P$, where P is the distance from the DCM to the sample. The size of the beam at the sample position can be approximated as wP', where w is the RMS value of the vertical beam divergence and P' is the distance from the X-ray source to the sample ($P' > P$). Typical values for the beam divergence are 5–20 µrad, which is much larger than the typical values for the vibrational amplitudes. Thus, the additional broadening of the direct beam due to the vibrations is small and typically less than 5%.

The effect of the crystal vibrations becomes significant in the case of focusing. It can be understood in the frame of geometrical optics as shown in Fig. 2. Here, we consider the optical setup including the DCM at distance z_m from the source and the thin lens with large aperture at distance z_o. The lens focal length f is such that the beam is focused at the image distance z_i after the lens, $1/f = 1/z_o + 1/z_i$. The DCM angular vibrations lead to the deviation of the beam from the central axis by an angle of $2\varphi_m$. The line which describes the beam propagation after the lens is defined by the deviations from the central axis at the lens position, x_l, and at the image position, x_i. The deviation at the lens position is $x_l = 2\varphi_m(z_o - z_m)$. The deviation at the image position can be

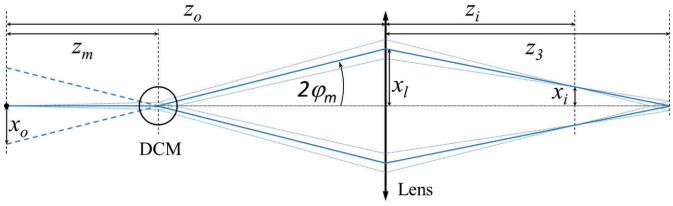

Figure 2
Diagram of the beam propagation through the optical system which includes the DCM which turns a beam by angle $\pm 2\varphi_m$ and the thin lens with large aperture and focal length f such that $1/f = 1/z_o + 1/z_i$.

calculated taking into account that the rotation of the beam by $2\varphi_m$ is equivalent to a shift of the virtual X-ray source by $x_o = -2\varphi_m z_m$. Then, taking into account the lens magnification rule, we obtain $x_i = -(z_i/z_o)x_o = (z_i/z_o)2\varphi_m z_m$.

Without vibrations the beam size at the image position is $s_i = (z_i/z_o)\,s_o$, where s_o is the vertical source size. The average over angular vibrations leads to the broadening of the beam size by x_i. Thus, the effect of the DCM angular vibrations can be estimated from the comparison of the beam size s_i and deviation x_i. These values are proportional to the source size, s_o, and deviation of the virtual X-ray source, $x_o = -2\varphi_m z_m$. The typical distance from the X-ray source to the DCM is z_m = 30–50 m and the characteristic amplitude of the angular vibrations is φ_m = 0.1–1 µrad. Thus, we obtain that $2\varphi_m z_m$ = 6–100 µm is comparable with or larger than the X-ray source size s_o = 5–20 µm, which means that the beam size at the image position is mostly defined by the angular vibrations.

The vibrations lead not only to an increase of the beam size but also to a shift of the image position. Indeed, as seen in Fig. 2, there is a position denoted by distance z_3 where the beam deviation from the central axis is zero independent of the amplitude of the vibrations. This position is the image position for the virtual source situated at the monochromator position, $1/f = 1/(z_o - z_m) + 1/z_3$. When the angular vibrations amplitude φ_m becomes sufficiently large, the smallest beam size, the image position, will be found not at z_i but at z_3. Thus, with increase of the vibration amplitude the position of the smallest beam size continuously moves from z_i to z_3. The distance z_3 can be either positive or negative depending on the distance from the monochromator to the lens. The largest effect is observed if $z_o - z_m$ is small and z_3 is negative and large. Such conditions often occur for long focal lenses used for pre-focusing of the X-ray beam.

2.1. Phase-space calculation

The analytical expression for beam broadening and shift of the image position due to the vibrations can be obtained using phase-space analysis (Pedersen & Riekel, 1991; Huang & Bilderback, 2001; Ferrero *et al.*, 2008) in the paraxial approximation. The optical setup presented in Fig. 2 is considered, which includes the X-ray source, the monochromator and the thin lens. Only the vertical transverse direction affected by the monochromator vibrations is considered, with coordinates x, θ being the linear and angular deviation from the central axis. The beam is assumed to be Gaussian with s_o and w_o being RMS values for the beam size and divergence at the source position, respectively. The thin lens has a focal length f $(1/f = 1/z_o + 1/z_i)$ and a fixed aperture of Gaussian shape with an aperture RMS value A. The angular beam vibrations are introduced by the coordinate transformation at the monochromator position as $(x', \theta') = (x, \theta) + [0, 2\varphi_m(t)]$. The beam propagation through the lens and free space are described by the conventional coordinate transformation of the phase-space approach. Then, applying coordinate substitution and integration over angular coordinate, we obtain the beam profile in vertical direction x at the distance z after the lens and at time t expressed as

$$I\big[x; \varphi_m(t)\big] = I_0 \exp\left\{ -\frac{\big[x - 2z_m\varphi_m(t)c(z)\big]^2}{2\sigma_0^2(z)} - \frac{4\varphi_m^2(t)(z_o - z_m)^2}{2(A^2 + B^2)} \right\}, \quad (3)$$

where $B = z_o w_o$ is the RMS value of the beam size at the lens position from the point source and I_0 is the normalization coefficient. $c(z)$ is the proportionality coefficient between $2z_m\varphi_m(t)$ and the deviation of the beam from the central axis, $\sigma_0(z)$ is the RMS value of the beam size,

$$c(z) = \frac{z}{z_o} - \frac{(z_o - z_m)(z - z_i)}{z_m z_i (1 + B^2/A^2)}, \quad (4)$$

$$\sigma_0^2(z) = s_o^2 \frac{z_i^2}{z_o^2} + \frac{(z/z_i - 1)^2}{(1/A^2 + 1/B^2)}. \quad (5)$$

Here and further we assume that $A^2 + B^2 \gg s_o^2$ which is valid in most cases.

It is clear from equation (5) that at any time t the smallest beam size is $\sigma_0 = s_o(z_i/z_0)$ at $z = z_i$. Equations (3) and (4) show that the shift of the beam center at z_i is $x_i = 2z_m\varphi_m(t)z_i/z_o$. These results are the same as those obtained from the simple geometrical consideration in the previous section.

The beam profile averaged over angular vibrations, $I(x)$, is obtained by integration of equation (3) over time T larger than characteristic periods of the vibrations,

$$I(x) = \frac{1}{T}\int_0^T \mathrm{d}t\, I\big[x; \varphi_m(t)\big]. \quad (6)$$

In general, this integration requires knowledge of the function $\varphi_m(t)$. We assume that the angular vibrations are completely stochastic. In this case, the integration over time can be replaced (Goodman, 2015) by the integration over φ_m with Gaussian probability having a RMS value σ_m as defined by equation (1),

$$I(x) = \int_{-\infty}^{\infty} \mathrm{d}t\, I(x; \varphi_m) \exp\left(-\frac{\varphi_m^2}{2\sigma_m^2}\right). \quad (7)$$

In reality, the DCM angular vibrations are not stochastic but rather harmonic with several eigenfrequencies. However, numerical integration of equation (6) with experimentally measured $\varphi_m(t)$ shows that the stochastic approximation of (7) works well. The only exception is the situation when $\varphi_m(t)$

describes a large oscillation at a single frequency, where the stochastic approximation does not work and $\varphi_m(t)$ has to be replaced by a cosine function.

Inserting (3) into (7) and performing analytical integration we obtain the final expression for the beam profile averaged over vibrations as

$$I(x) = I_0' \exp\left[-\frac{x^2}{2\sigma(z)^2}\right], \tag{8}$$

where I_0' is the normalization parameter. The RMS value of the beam size $\sigma(z)$ is written as

$$\sigma(z)^2 = \sigma_0(z)^2 + \left[2\sigma_m z_m c(z)\right]^2 \left\{1 + \frac{\left[2\sigma_m(z_o - z_m)\right]^2}{A^2 + B^2}\right\}^{-1}. \tag{9}$$

Simulation of $\sigma(z)$ *versus* distance z after the lens is shown in Fig. 3 for different values of the vibration amplitude σ_m and for two optical setups with long-focal-length lens situated close to the monochromator (Fig. 3*a*) and with short-focal-length lens situated close to the sample (Fig. 3*b*). In both cases the broadening of the beam size at the image position is observed. The shift of the image position is strong and negative for the first setup and small and positive for the second setup.

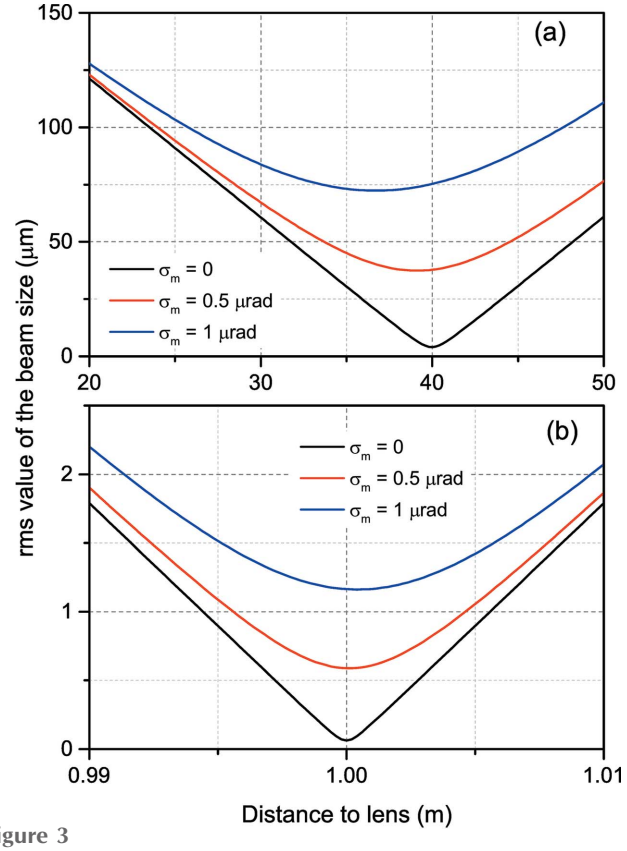

Figure 3
Simulation of the beam size RMS value *versus* distance after the lens for different amplitudes of the DCM angular vibrations σ_m for (*a*) the long-focal-length lens with z_o = 50 m, z_i = 40 m, A = 1000 μm; (*b*) the short-focal-length lens with z_o = 80 m, z_i = 1 m, A = 200 μm. For both figures the DCM is at z_m = 47 m, X-ray source RMS size and divergence are s = 5 μm, w = 5 μrad, respectively.

The simple analytical expression for the smallest beam size σ_{min} and shift of the image position z_{min} can be derived using the approximation of small σ_m. In this case we obtain

$$\sigma_{min} = \frac{z_i}{z_o}\left[s_o^2 + (2z_m\sigma_m)^2\right]^{1/2}, \tag{10}$$

$$\frac{z_{min} - z_i}{z_i} = -(2\sigma_m z_m)^2\left[\frac{1}{A^2}\frac{z_i^2}{z_o^2} + \frac{1}{B^2}\left(\frac{z_i^2}{z_o^2} + \frac{z_i}{z_o} - \frac{z_i}{z_m}\right)\right]. \tag{11}$$

Thus, the broadening of the beam size is expressed *via* broadening of the X-ray source size due to the virtual source shift by $2z_m\sigma_m$ and proportional to the RMS value of the vibrations and to the distance from the X-ray source to the DCM. The effect of the DCM angular vibrations will be negligible when $s_o > 2z_m\sigma_m$. Taking z_m = 40 m and s_o = 5 μm, the values typical of the PETRA III light source, we find that the beam performance will not be deteriorated by vibrations if $\sigma_m < 0.06$ μrad.

The sign of the image position shift in equation (11) is negative when z_i/z_o is sufficiently large, *i.e.* for the long-focal-length lens. The shift increases for a smaller lens aperture or smaller beam divergence and for a larger ratio of z_i/z_o.

3. Experimental measurements of angular vibrations

The experimental setup for angular DCM vibration measurements should be sensitive enough to measure vibrations with RMS values down to at least 0.05 μrad. In addition, the cut-off frequency should be of the order of 300–1000 Hz in order to resolve fast vibrations, which exist for certain types of DCM. We have measured vibrations using the setup shown in Fig. 4 including compound refractive lenses (CRL) or mirrors, which focus the X-ray beam, a knife-edge installed at the beam center and a PIN photodiode or an ionization chamber as a detector. The signal in the detector is amplified and measured with an oscilloscope with cut-off frequency of 5 kHz. Two types of measurements are performed. In the first measurement the flux in the detector is measured as a function of time using an oscilloscope. In the second measurement the average over the time signal is detected as a function of the angle of the second DCM crystal, θ. The comparison of the results of the measurements allows one to transform the intensity scale to the angular scale and calculate an RMS value

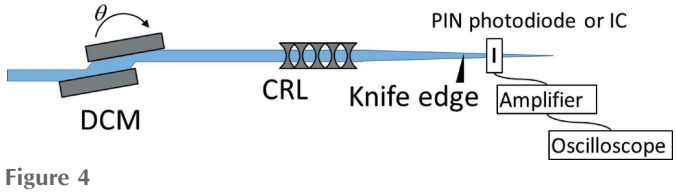

Figure 4
Experimental setup for the measurements of the DCM angular vibrations including DCM, compound refractive lenses (CRL), knife-edge at the beam center and PIN photodiode or ionization chamber (IC). The signal from the PIN photodiode is amplified and measured by an oscilloscope.

of the angular vibrations. The validity of this method is explained as follows.

According to equation (3) the instant beam profile at position z after the lens can be presented *via* the function $I(x, t) = f\{x - a[\theta + \varphi_m(t)]\}$ where $f(y)$ is the peak function [Gaussian function in equation (3)], x is the vertical coordinate, θ is the deviation of the motor angle of the second crystal out of equilibrium and a is the proportionality coefficient. The total intensity after the knife-edge is the integral of the beam profile $J(x, t) = F\{x - a[\theta + \varphi_m(t)]\}$. An expansion up to the linear term gives $J(x, t) = F(0) - a[\theta + \varphi_m(t)]f(0)$. The time scan measured by the oscilloscope at $\theta = 0$ is presented as $J(t) = F(0) - a\varphi_m(t)f(0)$. The angular scan is calculated using a time average, which leads to $J(\theta) = F(0) - a\theta f(0)$, where we take into account that $\langle\varphi_m(t)\rangle = 0$. Thus, the linear parts in both scans have the same proportionality coefficients between flux and angle leading to the possibility to correlate these values. The proportionality coefficient depends on the distance between image position and knife-edge position. By changing this distance the sensitivity of the measurements can be tuned.

The experimental test of the angular vibrations measurements has been performed at beamline P06 of PETRA III light source. The setup includes a DCM at 35 m from the X-ray source, a compound refractive lens with 400 µm aperture at 48 m from the source and a knife-edge at 90 m from the source with a PIN photodiode downstream of the blade. The measurements were performed with the same compound refractive lens at 17.5 keV where the image position is at the knife-edge position with beam size around 60 µm and at 18.5 keV where the image position shifted downstream by ∼8 m and the beam size measured by the knife-edge increases to 120 µm. A combination of the time and angular scans for these energies is shown in Figs. 5(*a*) and 5(*b*). The amplitude of the flux oscillations becomes smaller when the knife-edge is out of the image position. However, the ratio between the amplitude of the flux oscillations and the gradient in the angular scan stays almost the same. Thus, almost the same RMS values of the angular vibrations are obtained in the two measurements at different energies with σ_m = 0.21 and 0.18 µrad, respectively.

Another way to measure the angular vibrations is to investigate the time dependence of the flux when one crystal of the DCM is moved to the rising/falling edge of the rocking curve (Chumakov *et al.*, 2014; Yamazaki *et al.*, 2013). The focusing device and knife-edge are not necessary in this case. However, a sharp edge is required in order to provide sufficient sensitivity of the method. The measurements have been performed at the same beamline using radiation passing through the DCM with Si(333) reflection at 52.5 keV. The unwanted 17.5 keV radiation was filtered by a Cu absorber. A comparison of the time dependence and angular scans of the rocking curve is shown in Fig. 5(*c*). Here, contrast of the time oscillations is smaller than in the previous measurements. This is due to the rocking-curve width which is five times larger than theoretically expected. Nevertheless, the obtained angular vibrations, σ_m = 0.23 µrad, reasonably agrees with the other measurements.

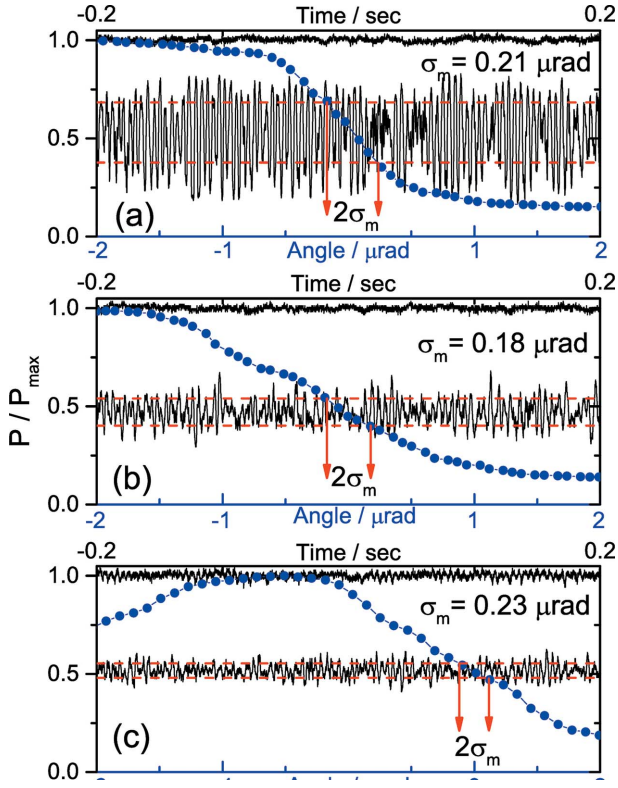

Figure 5
Vibration measurements performed with (*a*, *b*) knife-edge and focused beam at (*a*) 17.5 keV and (*b*) 18.5 keV, (*c*) at the falling edge of the rocking curve at 52.5 keV. The blue circles show the average flux *versus* angle of the second DCM crystal (bottom axes), the solid black lines show flux oscillations *versus* time (top axes). The dashed lines show the RMS deviation of these oscillations from equilibrium which are converted to the angular scale as shown by the arrows. The solid black lines with average value around 1 show the flux oscillation without knife-edge (*a*, *b*) and at the maximum of the rocking curve (*c*) which practically demonstrate the noise oscillations.

Thus, three independent measurements reproduce the RMS value of the angular vibrations with a precision of 10%. The results can be further verified looking at the frequency distributions of the vibrations. Fig. 6 shows the amplitude spectral density of the vibrations, $|a(\nu)|$, obtained *via* Fourier transformation of the time spectra and normalized as $\int_0^{\nu_{max}} d\nu\, |a(\nu)|^2 = \sigma_m^2$. All three distributions show the same characteristic features in the frequency range up to 800 Hz.

Both methods to measure angular vibrations presented above have advantages and drawbacks. The measurements using the DCM rocking curve require a sharp edge which can be only obtained using reflections higher than Si(111) at high energies. The sufficient sharpness sometimes cannot be obtained due to the imperfection of the DCM crystals. Moreover, the energies above ∼40 keV required here sometimes are not available at the beamline. On the other hand, the measurements using a focusing device can give incorrect results if vibrations of the focusing device or knife-edge are present. Accurate measurements require a combination of the different approaches where comparison of the spectral densities allows for the separation of the non DCM vibrations.

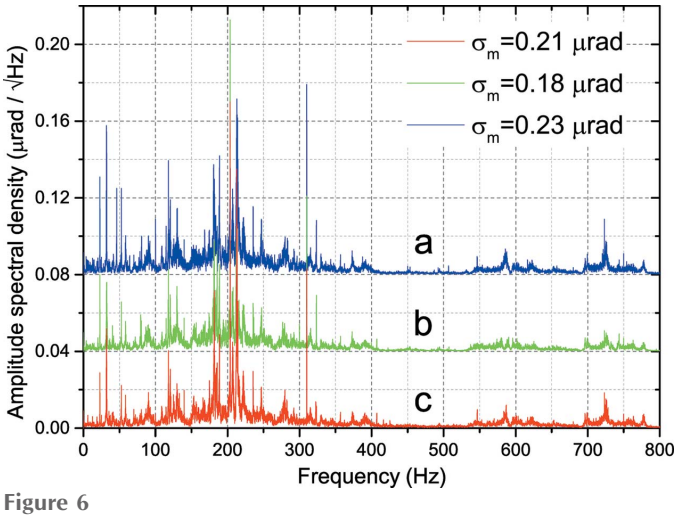

Figure 6
Amplitude spectral density of the DCM angular vibrations obtained by three different measurements shown in Fig. 5 shifted by 0.04 in vertical scale for visibility. Labels (*a*, *b*, *c*) correspond to the labels in Fig. 5.

4. Angular vibrations of the DCMs installed at PETRA III light source

The methods presented in the previous section have been applied to measure angular vibrations of the DCM installed at the beamlines of the PETRA III light source. These are liquid-nitrogen-cooled DCMs (FMB Oxford, Osney Mead, UK), which are equipped with two pairs of crystals [typically Si(111) and Si(311) reflections] with a fixed offset of the reflecting beam of 20–24 mm. The first- and second-crystal cages are mounted on the common back-plate, which is rotated in order to change the Bragg angle using a direct-drive goniometer developed by FMB Oxford (Kristiansen *et al.*, 2015). The Bragg angle is measured by an optical rotary ring encoder mounted onto the rotary axis of the goniometer. The electrical currents inside a three-phase direct-drive motor are commutated to keep the angle stable and to move to different angles, respectively. The position is controlled by a cascaded feedback loop working at update frequencies of several kHz. Both crystals are cryogenically cooled using a cryocooler, which pumps liquid nitrogen through Cu blocks clamping the crystals. The cryostat has a low-pressure liquid-nitrogen bath, which cools the high-pressure circuit. Inside the high-pressure reservoir the static pressure (up to 5 bar) is controlled by a heater. The pressure to feed the cryolines going to the monochromator is provided by a Barber–Nichols pump inside the high-pressure circuit.

The measurements were performed at the beamlines P01, P02, P03, P06, P09, P10 and P11 at energies of 9–25 keV and with the Si(111) reflection. The frequency of the cryocooler pump was in the range 16–25 Hz and the pressure in the range 1.5–3 bar. The RMS values of the angular vibrations are shown in Table 1. The vibrations were measured in the frequency range up to 1 kHz. The relative error of the measurements has been estimated to be 25% of the set of independent measurements of the vibrations performed at beamline P01 during half a year. The amplitude of the vibrations can significantly change depending on the cryocooler pump frequency and pressure, the relative positions of the crystals inside the DCM which is defined by the selected energy and the feedback loop system conditions. Thus, in general, we can say that the characteristic RMS amplitudes of the DCM angular vibrations observed for the DCMs installed at PETRA III light source vary between 0.1 and 0.3 μrad with an average value of 0.2 μrad. Using the distance from the X-ray source to the DCM, the broadening of the source size due to the vibrations is calculated according to equation (10) and presented in Table 1. The broadening varies between 9 and 23 μm, which is significantly larger than the RMS value for the X-ray source size of 5 μm. Thus, the effect of the vibrations on the beam size at the image position has to be taken into account together with other reasons for the beam deterioration.

Table 1
The characteristic DCM vibration RMS value, σ_m, measured in the frequency range up to 1 kHz, the distance from X-ray source to DCM, z_m, and the source broadening due to the vibrations, $2z_m\sigma_m$, for the DCM installed at several beamlines of PETRA III light source.

	P01	P02	P03	P06	P09	P10	P11
σ_m (μrad)	0.20	0.10	0.17	0.20	0.23	0.30	0.21
z_m (m)	47	44	53	35	47	38	40
$2z_m\sigma_m$ (μm)	19	9	18	14	22	23	17

The improvement of the mechanical stability by replacing the liquid-nitrogen tubes and components of the DCM by more stable pieces and changing of the DCM operation scheme by switching off the feedback loop control system reduce vibrations down to 0.1 μrad or more as have been seen after upgrade of DCMs at beamlines P02 and P11 (Doehrmann, 2016). Also, the vibrations have been significantly suppressed at beamline P10 by installation of the channel-cut crystal in parallel to two independent crystals (Zozulya *et al.*, 2014) with RMS value of the vibrations less than 0.05 μrad. Our results for the DCM angular vibrations are comparable with RMS value 0.1 μrad measured for the new FMB Oxford DCM (Kristiansen *et al.*, 2015) and with 0.11 μrad reported for the DCM installed at beamline ID18 at ESRF (Chumakov *et al.*, 2014).

The amplitude spectral density of the vibrations measured at P01, P02, P06 and P09 is shown in Fig. 7. While the beamlines are equipped with the same type of monochromator, the vibrational spectra are different. This difference is related to the type of DCM operation at particular beamlines and to the deterioration of the mechanical components with time. The remarkable feature of the measured vibrations is that there is significant contribution up to at least 300 Hz. Thus, a measurement setup with high cut-off frequency is a crucial requirement in order to measure all vibrations. Taking, for example, 150 Hz as a cut-off frequency, one accounts only for 50% of the vibrations for the DCM at beamline P02 and only 5% for the DCM at beamline P06. As shown by the off-beam vibration measurements (Kristiansen *et al.*, 2015; Doehrmann, 2016), the vibrations below and above ∼150 Hz have different origins. The low-frequency vibrations are induced mainly by

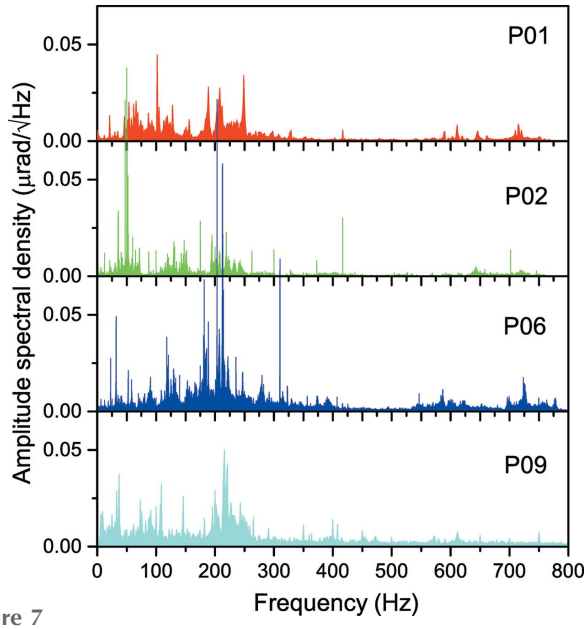

Figure 7
Amplitude spectral density of the DCM angular vibrations measured at several beamlines of PETRA III light source.

the liquid-nitrogen flow. On the other hand, the presence of high-frequency contributions is related to the high-frequency oscillations of the feedback loop. The analysis of the amplitude spectral density is helpful in order to find weak points of the DCM hardware and to further improve these components.

Another result coming from the analysis of the amplitude spectral density is a small contribution to the vibrations at the frequency range below 25 Hz. Vibrations in this frequency range are typical for X-ray optical devices due to ground vibrations. The small amount of such vibrations in Fig. 7 is related to the coupling of both crystals to the same back-plate which shows the usefulness of this approach.

5. Conclusion

Here, we presented a theoretical description of the effect of monochromator angular vibrations on the properties of the focused beam. It is shown that both size of the beam and image position are affected by vibrations. The broadening of the beam size is described by the broadening of the virtual X-ray source by $2\sigma_m z_m$, which is proportional to the characteristic RMS value of the angular vibrations and to the distance of the X-ray source to the monochromator.

Experimental methods were described, which give the possibility to measure monochromator angular vibrations in a broad frequency range with high sensitivity. The combination of different methods is important in order to separate unwanted contributions coming from other optical devices in the beam.

The methods have been applied to characterize a set of monochromators of the same type installed at the PETRA III light source. It was found that the RMS value of the vibrations varies between 0.1 and 0.3 μrad leading to the broadening of the X-ray source of the order of 9–23 μm. These values are larger than the vertical size of the X-ray source, being ∼5 μm. Thus, the vibrations lead to a significant deterioration of the X-ray beam quality. Efforts are ongoing in order to decrease the amplitude of the monochromator angular vibrations below 0.1 μrad.

Acknowledgements

We are grateful to the staff of the PETRA III beamlines P01, P02, P03, P06, P09, P10, P11 and the FS-BT vacuum group helping to perform the measurements and providing the infrastructure to work on the DCM hardware, respectively.

References

Bilderback, D. H., Freund, A. K., Knapp, G. S. & Mills, D. M. (2000). *J. Synchrotron Rad.* **7**, 53–60.
Chumakov, A., Rüffer, R., Leupold, O., Celse, J.-P., Martel, K., Rossat, M. & Lee, W.-K. (2004). *J. Synchrotron Rad.* **11**, 132–141.
Chumakov, A. I., Sergeev, I., Celse, J.-P., Rüffer, R., Lesourd, M., Zhang, L. & Sánchez del Río, M. (2014). *J. Synchrotron Rad.* **21**, 315–324.
Doehrmann, R. (2016). To be published.
Ferrero, C., Smilgies, D.-M., Riekel, C., Gatta, G. & Daly, P. (2008). *Appl. Opt.* **47**, E116–E124.
Goodman, J. W. (2015). *Statistical Optics*. New York: John Wiley & Sons.
Hinebaugh, J., Challa, P. R. & Bazylak, A. (2012). *J. Synchrotron Rad.* **19**, 994–1000.
Huang, R. & Bilderback, D. H. (2001). *Nucl. Instrum. Methods Phys. Res. A*, **467–468**, 978–981.
Huang, R., Bilderback, D. H. & Finkelstein, K. (2014). *J. Synchrotron Rad.* **21**, 366–375.
Kristiansen, P., Horbach, J., Döhrmann, R. & Heuer, J. (2015). *J. Synchrotron Rad.* **22**, 879–885.
Pedersen, J. S. & Riekel, C. (1991). *J. Appl. Cryst.* **24**, 893–909.
Rutishauser, S., Rack, A., Weitkamp, T., Kayser, Y., David, C. & Macrander, A. T. (2013). *J. Synchrotron Rad.* **20**, 300–305.
Uhlén, F., Rahomäki, J., Nilsson, D., Seiboth, F., Sanz, C., Wagner, U., Rau, C., Schroer, C. G. & Vogt, U. (2014). *J. Synchrotron Rad.* **21**, 1105–1109.
Yamazaki, H., Ohashi, H., Senba, Y., Takeuchi, T., Shimizu, Y., Tanaka, M., Matsuzaki, Y., Kishimoto, H., Miura, T., Terada, Y., Suzuki, M., Tajiri, H., Goto, S., Yamamoto, M., Takata, M. & Ishikawa, T. (2013). *J. Phys. Conf. Ser.* **425**, 052001.
Zhang, L., Sánchez del Río, M., Monaco, G., Detlefs, C., Roth, T., Chumakov, A. I. & Glatzel, P. (2013). *J. Synchrotron Rad.* **20**, 567–580.
Zozulya, A. V., Shabalin, A., Schulte-Schrepping, H., Heuer, J., Spiwek, M., Sergeev, I., Besedin, I., Vartanyants, I. A. & Sprung, M. (2014). *J. Phys. Conf. Ser.* **499**, 012003.